USB Proceedings

2015 IEEE International Electric Machines and Drives Conference (IEMDC)

Coeur d'Alene Resort
Coeur d'Alene, ID, U.S.A.
11 - 13 May, 2015

Sponsored by

The Institute of Electrical and Electronics Engineers (IEEE)
IEEE Industrial Electronics Society (IES)

Co-sponsored by

IEEE Power and Energy Society (PES)
IEEE Industry Applications Society (IAS)
IEEE Power Electronics Society (PES)

IEEE Catalog Number: CFP15EMD-USB
ISBN: 978-1-4799-7940-0

Loss minimizing control strategy for electrical machines considering iron loss distribution

Andreas Ruf, Andreas Thul, Simon Steentjes, Kay Hameyer
Institute of Electrical Machines
RWTH Aachen University
Aachen 52062, Germany
Email: Andreas.Ruf@iem.rwth-aachen.de

***Abstract*—Iron losses have a large share in the overall losses of high power density electrical machines operating as variable speed drives. Therefore, commonly used control strategies such as Maximum Torque per Ampere or Maximum Torque per Voltage aiming at minimizing the copper losses do not select the best direct- and quadrature currents to maximize the efficiency or minimize the overall losses at each operating point. This paper elaborates a loss minimizing control strategy considering the iron loss distribution at all operating points, comparing different iron loss models.**

***Index Terms*—Loss minimization, efficiency optimization, field oriented vector control, nonlinear optimization**

I. Introduction

Permanent-magnet synchronous machines (PMSM) are used in electrical drive trains requiring high power density and high efficiency in a wide operating range. Especially PMSM with buried magnets offer high power densities and low rotor losses. The magnetic salience leads to a reluctance torque which can be used applying the best direct and quadrature (dq) current combination to maximize the torque per ampere (MTPA). This results in minimal copper losses and is a common choice. However, in high power density machines operating as variable speed drives iron losses have a large share in various operating points due to high magnetic utilization and elaborated field frequencies. On that account, the iron losses need to be considered in all operating points to select the best direct and quadrature current combination leading to the lowest overall losses. For this purpose the iron loss calculation scheme is of particular interest. This loss minimizing control strategy is known as the maximum efficiency (ME) control, whose theory is well known and has been proposed and applied by different authors [1]–[3].

A commonly used approach to represent the variability of the iron losses is to add a speed-dependent iron loss equivalent resistance to the machine model [1], [2], [4]–[7] or to employ variable loss coefficients [8] and elementary iron loss models [9]–[13]. All of these approaches solely consider iron losses caused by the fundamental harmonic of the magnetic flux density in the machine leading to a strong simplification, in particular in the field-weakening range.

The main challenge and central task of the loss minimizing control strategy is an accurate description of the considered loss components maintaining the simplicity of the loss models to be applicable for real-time applications. Depending on whether or not a prototype exists the loss models are parametrized by measurements [11], [14] or directly look-up tables of measured losses are used to accomplish the simplicity and accuracy [8]. Considering the speed-dependent additional losses during the control of the machine enable to minimize the overall losses, tantamount to maximizing the efficiency. For PMSM especially at the partial load area the efficiency can be improved, because at this area the iron losses are dominant. Considering the drive cycles of speed-variable traction drives in [8] and [14] show that the average efficiency gain or energy loss decrease rises up to $2\,\%$, which is a non-negligible amount that can be achieved by the correct control of the machine.

This paper deals with the same methodical approach to minimize the overall losses, but in contrast to other investigations this paper bases the iron loss estimation solely on standardized Epstein measurement data to parametrize the applied iron loss models in combination with a Finite-Element model and specific control strategy to incorporate the operation characteristics of the machine. This approach allows combining efficiently the material information gained from standardized measurements (loss and non-linear magnetization behavior) and the operation dependent load characteristics. Therewith, an *a priori* design and loss prediction of the machine across the whole torque-speed map is possible. The importance of the used iron loss model and the comparison with measured data is discussed in detail. This paper uses two extended iron loss models [15] in combination with Finite-Element simulations to derive a more accurate loss minimizing control strategy. These two extended iron loss models share an additional eddy-current loss component to account for increased iron losses at high magnetic flux densities and high excitation frequencies. They are different in terms of the consideration of higher harmonic flux density component and the hysteresis loss component.

II. Modeling approach

A. Machine model

In order to evaluate the proposed methodology a permanent magnet synchronous (PMSM) machine with buried magnets is modeled in a rotor-flux-fixed dq-reference frame including cross coupling magnetization and saturation [16]:

$$\begin{bmatrix}\hat{\Psi}_\mathrm{d}\\ \hat{\Psi}_\mathrm{q}\end{bmatrix} = \begin{bmatrix}L_\mathrm{dd} & L_\mathrm{dq}\\ L_\mathrm{qd} & L_\mathrm{qq}\end{bmatrix}\begin{bmatrix}\hat{i}_\mathrm{d}\\ \hat{i}_\mathrm{q}\end{bmatrix} + \begin{bmatrix}\hat{\Psi}_\mathrm{f,d}\\ \hat{\Psi}_\mathrm{f,q}\end{bmatrix}. \tag{1}$$

978-1-4799-7940-0/15/$31.00 ©2015 IEEE

The quadrature and direct current is varied during simulation to extract the torque calculated by the eggshell method for different excitations [17]. The average torque is determined by the formula:

$$T = \frac{3}{2} p \left(\hat{\Psi}_{\mathrm{d}} \hat{i}_{\mathrm{q}} - \hat{\Psi}_{\mathrm{q}} \hat{i}_{\mathrm{d}} \right) \tag{2}$$

To calculate the efficiency of the machine, the various loss components which occur during the operation have to be considered. These are detailed in the following subsections.

B. Copper loss model

For the consideration of the copper or ohmic losses the equation:

$$P_{\mathrm{Cu}} = 3 R_{\mathrm{s}}(\theta) i_{\mathrm{eff}}^2$$

is used. The influence of the changing temperature of the stator windings is taken into account by using a temperature dependent stator resistance $R_{\mathrm{s}}(\theta)$, which is calculated by:

$$R_{\mathrm{s}}(\theta) = R_{\mathrm{s}}(\theta_0) \frac{1}{1 - (\theta - \theta_0) \cdot 3.9 \cdot 10^{-3} \ (\mathrm{deg}\, C)^{-1}} \tag{3}$$

The resistance $R_{\mathrm{s}}(\theta_0)$ is determined by a DC measurement at temperature θ_0 and for the simulation results set to a fixed value at temperature $\theta = 100\,^{\circ}\mathrm{C}$. Comparing the simulation results with measurement amounts to the temperature, measured at different points at the winding, is considered. Additional copper losses due to eddy currents and inverter loss are not taken into account.

C. Iron loss model

The utilized iron loss model [15] plays a central role for this control strategy. The model has to deliver reliable and accurate results in all operating points of the machine, i.e., material saturation characteristics, rotational iron losses and harmonics need to be considered. Therewith the loss distribution can be calculated and the control strategy adjusted. In this paper, two different iron loss calculation methods are applied. The first one calculates the iron losses solely based on the fundamental component of the magnetic flux density B_1 in combination with the fundamental frequency f_1. More precisely, the Fourier summations in (5) to (8) are replaced by the fundamental components. The second approach considers the influence of induced field harmonics using a Fourier series representation of the magnetic flux density waveform for the least common multiple of an electrical period and the rotational period of the rotor. Based on this, the amplitudes and orders of the field harmonics can be used for the iron loss calculation [18]–[20]. The level of magnetic flux distortion and rotational magnetization are included in both models in a similar way using the maximal and minimal magnetic flux densities B_{max}, i.e., B_{min}, over the Finite-Elements of the machine model during one magnetic period.

$$P_{Fe} = P_{\mathrm{hyst}} + P_{\mathrm{classical}} + P_{\mathrm{excess}} + P_{\mathrm{sat}} \tag{4}$$

with the following loss contributions:

$$P_{\mathrm{hyst}} = a_1 \left(1 + \frac{B_{\mathrm{min}}}{B_{\mathrm{max}}} \left(r_{\mathrm{hyst}} - 1 \right) \right) B_{\mathrm{max}}^{\alpha} f_1 \tag{5}$$

$$P_{\mathrm{classical}} = a_2 \sum_{n=1}^{\infty} \left(B_{\mathrm{n}}^2 \left(nf \right)^2 \right) \tag{6}$$

$$P_{\mathrm{excess}} = a_5 \left(1 + \frac{B_{\mathrm{min}}}{B_{\mathrm{max}}} (r_{\mathrm{excess}} - 1) \right) \sum_{n=1}^{\infty} \left(B_{\mathrm{n}}^{1.5} \left(nf \right)^{1.5} \right) \tag{7}$$

$$P_{\mathrm{sat}} = a_2 a_3 B_{\mathrm{max}}^{a_4 + 2} f_1^2 \tag{8}$$

The material dependent parameters ($a_1 - a_5$ and α) of the iron loss model (Table I) are identified using standardized Epstein measurement data (purely sinusoidal magnetic flux density waveforms). A comparison of loss predictions and measurements is depicted in Fig. 1.

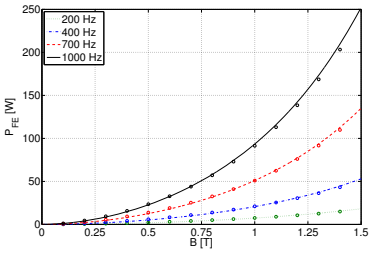

Fig. 1. Comparison of calculated iron losses with measurements at different frequencies using parameters of Table I for material grade M330-35A.

TABLE I
IRON LOSS MODEL COEFFICIENTS FOR THE INVESTIGATED ELECTRICAL STEEL, CLASSIFIED AS M330-35A.

α	a_1	a_2	a_3	a_4	a_5
2.0	$18.531e^{-3}$	$62.75e^{-6}$	$32.55e^{-3}$	5.0	$0.4e^{-3}$

D. Bearing loss model

The losses due to friction occurring in the shaft bearings are modeled by using an analytic approach described in [21]:

$$P_{\mathrm{bear}} = n_{\mathrm{bear}} f_0 \left(v_{\mathrm{bear}} n \right)^{\frac{2}{3}} d_{\mathrm{bear}}^3 \cdot 2\pi n \cdot 10^{-7},$$

where n_{bear}, f_0 and v_{bear} denominate the number of bearings, the bearing coefficient and the bearing viscosity. Values for f_0 and v_{bear} are taken for the data sheets provided by the bearing manufacturer. They are both temperature dependent are set to a mean value depending on the operating conditions.

III. Model-based control strategies

In order to calculate the operation points for the entire operating range a combined control strategy is used. The optimization problem is defined by:

$$\begin{aligned} \underset{\hat{i}_{\mathrm{d,i,j}}, \hat{i}_{\mathrm{q,i,j}} \in \mathbb{R}}{\text{minimize}} \quad & \mathrm{J}(\hat{i}_{\mathrm{d,i,j}}, \hat{i}_{\mathrm{q,i,j}}) = \sqrt{\hat{i}_{\mathrm{d,i,j}}^2 + \hat{i}_{\mathrm{q,i,j}}^2} \\ \text{subject to} \quad & T_{\mathrm{i}} = \frac{3}{2} p \left(\hat{\Psi}_{\mathrm{d,i}} \hat{i}_{\mathrm{q,i}} - \hat{\Psi}_{\mathrm{q,i}} \hat{i}_{\mathrm{d,i}} \right), \quad \forall\, i = 1, \ldots, m, \\ & \hat{u}_{\mathrm{j}} = \omega_{\mathrm{j}} \hat{\Psi}_{\mathrm{d,i}} \leq \hat{u}_{\mathrm{max}}, \qquad \forall\, j = 1, \ldots, n. \end{aligned}$$

with the torque vector $T_1, T_2, ..., T_\mathrm{m}$ subject to $m \in \mathbb{N}$ and the speed vector $n_1, n_2, ..., n_\mathrm{n}$ with $n \in \mathbb{N}$. This optimization problem combines the maximum torque per ampere (MTPA) control for the base speed range and the maximum torque per voltage (MTPV) control for the field weakening range. This control strategy minimizes the current vector, which is tantamount to minimized ohmic losses. Since the current amplitudes are known, which is the case for current driven controls, this control scheme is a simple method to reduce the losses and maximize the efficiency. However, this control strategy neglects the other losses, which are influenced by the direction and amplitude of the current vector. Du to the current-dependent magnetic field distribution the iron losses are also dependent on the position of the current vector for each occurring frequency. For this reason the iron losses can be considered in the control strategy by:

$$\begin{aligned} \underset{\hat{i}_{\mathrm{d,i,j}}, \hat{i}_{\mathrm{q,i,j}} \in \mathbb{R}}{\text{minimize}} \quad & \mathrm{J}(P_{\mathrm{Loss,i,j}}) = P_{\mathrm{Cu,i,j}} + P_{\mathrm{Fe,i,j}} \\ \text{subject to} \quad & T_i = \frac{3}{2} p \left(\hat{\Psi}_{\mathrm{d,i}} \hat{i}_{\mathrm{q,i}} - \hat{\Psi}_{\mathrm{q,i}} \hat{i}_{\mathrm{d,i}} \right), \quad \forall\, i = 1, \ldots, m, \\ & \hat{u}_\mathrm{j} = \omega_\mathrm{j} \hat{\Psi}_{\mathrm{d,i}} \leq \hat{u}_{\max}, \qquad\qquad \forall\, j = 1, \ldots, n. \end{aligned}$$

This optimization problem combines the maximum torque per loss (MTPL) control or the maximum efficiency control (ME) for the base speed range and the maximum torque per voltage (MTPV) control for the field weakening range and it has the same boundary conditions as the MTPA control.

IV. Results

A. Simulation Results

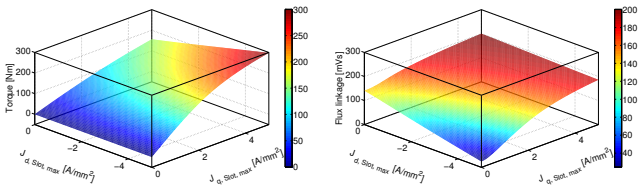

(a) Average torque vs. $\hat{i}_\mathrm{d}, \hat{i}_\mathrm{q}$. (b) Flux linkage vs. $\hat{i}_\mathrm{d}, \hat{i}_\mathrm{q}$.

Fig. 2. Torque and flux-linkage in dq-reference frame.

Figure 2 presents the result of the calculated average torque and flux-linkage for different dq-current excitations using Finite-Element simulation. In the case of a PMSM with buried magnets it is shown that the torque and the flux is strongly depend on the magnitude and angle of the rotor-flux-fixed current vector. This current-dependent data can be used by the first control strategy to calculate the speed-torque depended operating points.

Figure 3 shows the trajectories of average electro-magnetic torque calculated with different current excitations. Further an overlapping mesh of calculated operating points, from $0\,\mathrm{Hz}$ to $400\,\mathrm{Hz}$ fundamental electrical frequency and $0\,\mathrm{Nm}$ and $190\,\mathrm{Nm}$ inner electro-magnetic torque, using the combined control strategy is mapped. The rotor-flux-fixed current vectors are defined for each operating point by the operation points,

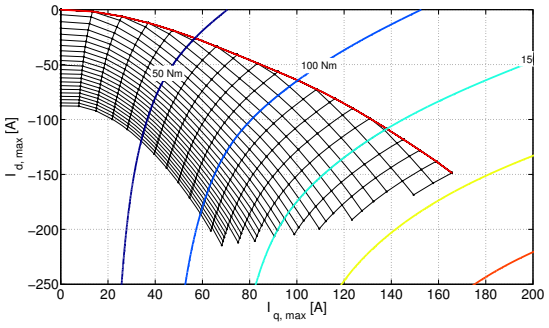

Fig. 3. MTPA-trajectory vs. $\hat{i}_\mathrm{d}, \hat{i}_\mathrm{q}$.

which are calculated for the given optimization problem. The basic speed range is represented by the trajectory that extends along the rising torques (red), whereas the field weakening area is represented by the mesh below this trajectory.

In comparison to these results, Fig. 4 presents the operating points for the overall loss minimizing MTPL control strategy. For the MTPA control all operation points for different frequencies in the base frequency range are on the MTPA-trajectory (red) until the voltage limit is reached, because only the current is considered and minimized by this strategy.

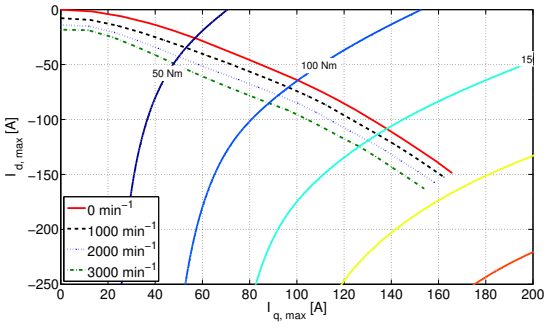

Fig. 4. MTPL-trajectory vs. $\hat{i}_\mathrm{d}, \hat{i}_\mathrm{q}$.

As soon as the voltage limit is reached the operating points are frequency-dependent due to the additional field weakening. This operation area is for both control strategies the same, because the voltage limit is in both cases the dominant factor or boundary and the point of minimum current as well as the point of minimum losses are out of the possible current excitations. The MTPL control strategy can exclusively be applied in the base speed range. In Figure 4 the MTPL-trajectories for four different velocities are presented. At standstill the trajectory corresponds to the MTPA-trajectory. With elevated speed the trajectories move to the negative d-axis, i.e., the field weakening to reduce the flux density and the occurring iron losses to accomplish the point of minimum losses.

Points of operation can be realized by different current excitations along the trajectories for given torques and speeds (Fig. 5 and 6).

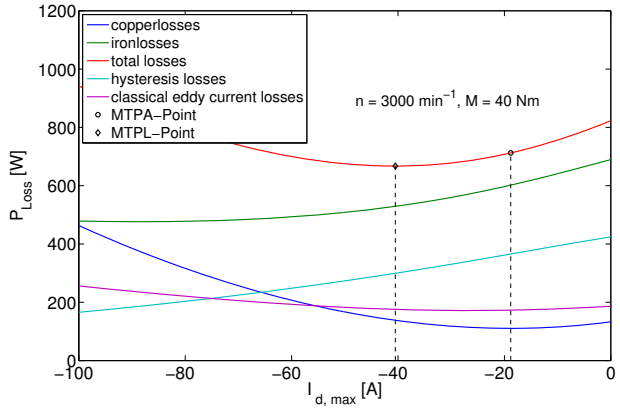

Fig. 5. Loss distribution versus the d-axis current ($n = 3000\,\mathrm{rpm}$).

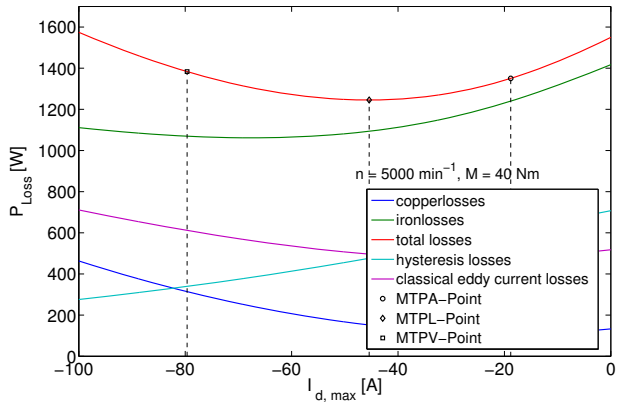

Fig. 6. Loss distribution versus the d-axis current ($n = 5000\,\mathrm{rpm}$).

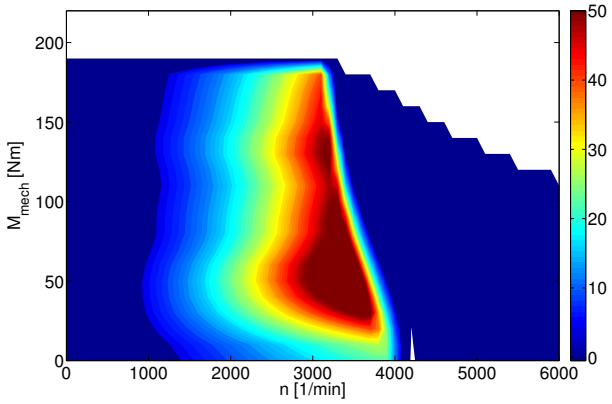

Fig. 7. Absolute reduced sum of losses in W using MTPL.

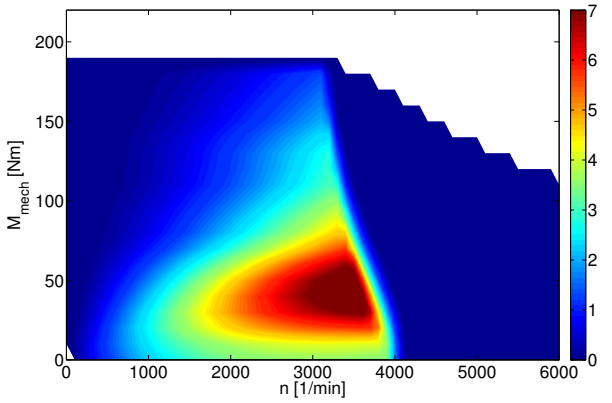

Fig. 8. Relative reduced sum of losses in % using MTPL.

It is apparent that the point of minimum losses is shifted to the direction of the negative d-axis. By decreasing the hysteresis loss by field weakening the higher field harmonics can cause an increase of eddy current losses, which need to be considered to minimize the overall losses. The result of reducing losses for all operation is presented in Fig. 7 and 8. The maximum reduction of losses is primarily dependent on the voltage limit, which is also shown in Fig. 6. As soon as the voltage limit is reached the MTPV criteria is the dominant factor for adjusting the dq-current combination.

Figure 8 presents the relative reduced sum of losses in % using the formula:

$$p_{\%} = \frac{P_{\mathrm{MTPA}} - P_{\mathrm{MTPL}}}{P_{\mathrm{MTPL}}}$$

The area just before the voltage limit is reached is the most influenced area by the loss minimizing strategy. In particular, the partial load area, where the iron losses are dominant, the efficiency is increased.

B. Experimental results

The machine under test (MUT) is a 8-pole synchronous machine with V-shape internal permanent magnets (IPMSM), dimensions and electrical parameters are given in table II. The test bench setup is shown in Fig. 9. The load machine (LM) is a speed controlled induction servo motor. A torque transducer TT (HBM T12) is coupled between the MUT and LM. The power analyzer (Yokogawa WT 1800) is used to

TABLE II
SIMULATION AND MACHINE PARAMETERS OF THE IPMSM.

Stator outer radius $r_{\mathrm{stator,o}}$	135 mm
Stator inner radius $r_{\mathrm{stator,i}}$	80.75 mm
Height of stator yoke h_{yoke}	40 mm
Radius of the middle of stator yoke N_{yoke}	125 mm
Air gap length δ	0.7 mm
Rotor outer radius $r_{\mathrm{rotor,o}}$	80 mm
Axial length l_{Fe}	90 mm
Number of Poles / Slots $2p/N$	8 / 48
Battery voltage U_{dc}	400 V
Rated current I_{N}	142 A
Rated torque M_{N}	162 Nm
Rated speed n_{N}	$2500\,\mathrm{min}^{-1}$
Rated power P_{N}	42.4 kW

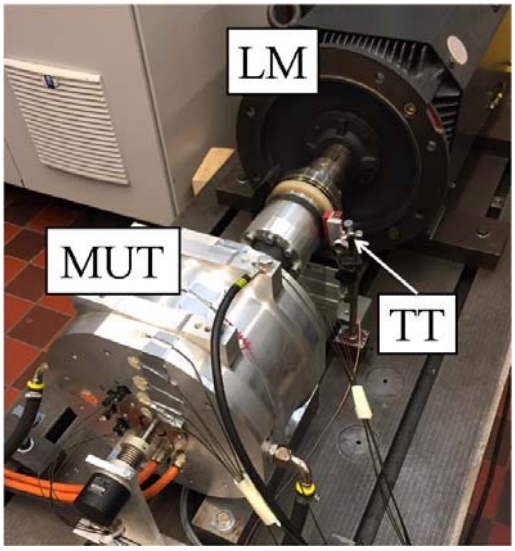

Fig. 9. Test bench setup.

calculate the electrical input power of the Aron circuit. The power analyzer additionally calculates the mechanical power transmitted between the MUT and LM using the TT. Thus the overall power losses in the MUT can be determined. As the iron losses cannot be measured directly, an accurate copper loss calculation is important for a proper iron loss separation. Therefore the temperature in the stator winding is measured at different positions to evaluate the average temperature.

Figure 10 presents the measured points (black) and the interpolated temperature in the end winding of the stator during the following analyzed measurement. By using equation 3 the temperature-dependent stator resistance value can be calculated for each measurement. In addition, the mechanical losses through bearings are calculated with equation II-D. Since these are small compared to the copper and iron losses, the mean measured temperature is used for approximating the bearing coefficients. Since the simulation results indicated that the maximum achievable loss reduction can be achieved for operating points located close to the maximum inverter voltage as shown in Fig. 7 and 8, a fixed speed of 3000 rpm is chosen. The reference speed is controlled by the load

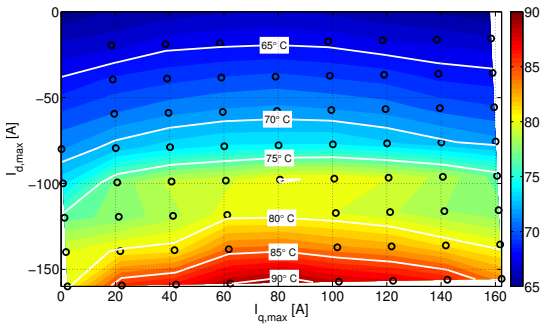

Fig. 10. Stator winding temperature during measurement.

machine. For the MUT a grid of reference values is defined in the dq-current plane, as indicated by the black dots in Fig. 10. For each quadrature current value the direct current is varied. To keep the temperature changes caused by high currents as small as possible, small and large reference current values are set alternately. As seen in Fig. 10, the temperature change during the measurement is limited to 30 K using this procedure. The change in rotor temperature, which affects a change in the permanent magnet flux density and further a change in the induced voltage, torque and iron losses. During the measurement the induced voltage is evaluated after each step in no load tests to keep the change in the voltage and temperature low. To avoid multiple FE simulations, the mean value of the measured induced voltage is used to adapt the flux linkage in the simulation.

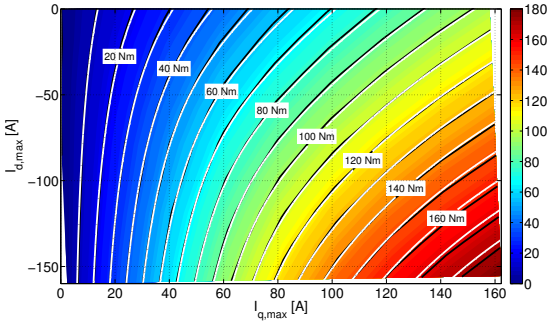

Fig. 11. Comparison of measured (black) and simulated (white) average torque.

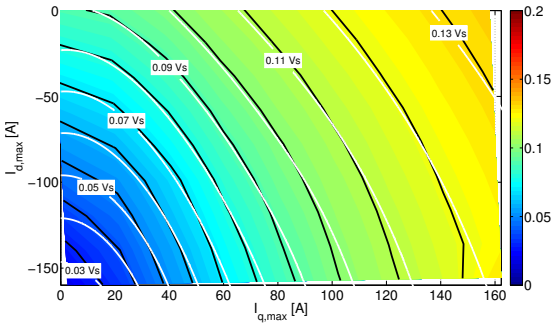

Fig. 12. Comparison of measured (black) and simulated (white) flux linkage.

Figures 11 and 12 present a comparison between measured (black) and simulated (white) torque and flux linkage values in the dq-reference current plane, which indicates a good correlation between the measured values and this simplification. In order to achieve a good match between the measured flux linkage and the simulation results, the machine model described in equation 1 must be extended by a leakage inductance. This leakage inductance is determined by parameter variation during post processing and set to the value $L_\sigma = 50\,\mu\text{H}$. The result of the adaption is shown in Fig. 12. This shows in the whole dq-reference plane a good match. After this adaption

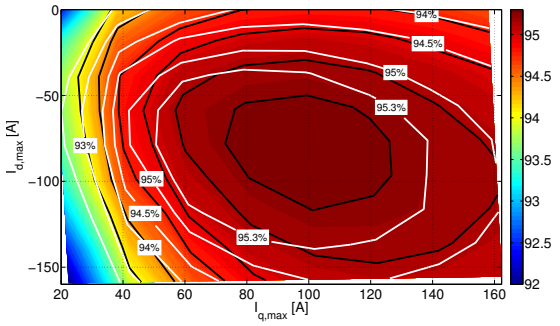

Fig. 13. Comparison of measured (black) and simulated (white) efficiency (without harmonics).

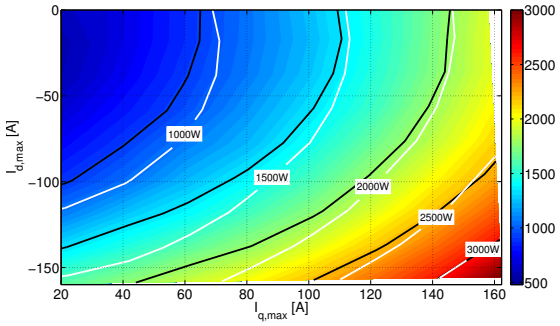

Fig. 14. Comparison of measured (black) and simulated (white) losses (without harmonics).

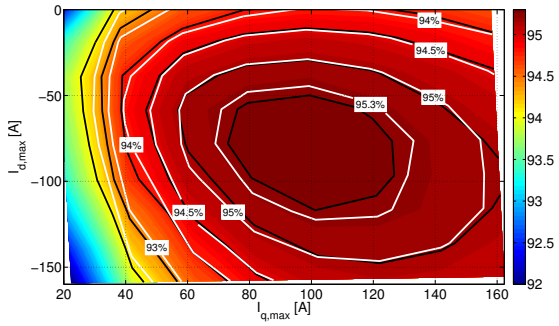

Fig. 15. Comparison of measured (black) and simulated (white) efficiency (including harmonics).

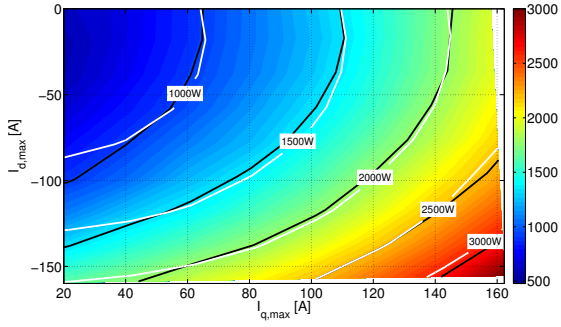

Fig. 16. Comparison of measured (black) and simulated (white) losses (including harmonics).

the machine can be controlled by the MTPA/MTPV control using the dq-current depended flux linkage and torque. For the loss minimizing control MTPL the losses must be known. For the copper loss model the stator resistance and the temporary winding temperature have to be measured and it is simple to calculate the ohmic losses occurring in the winding. For higher electric frequencies additional losses by eddy currents have to be considered in this model. The knowledge about the temporary occurring iron losses is not as simple. In this paper to models are used to compare the utility for the loss minimizing control. As described the two models are parameterized by measurements at the Epstein frame. In order to determine the losses occurring in the machine the difference between the supplied electric power and the mechanical power is calculated. The measured efficiency (black) is presented for $3000\,\mathrm{rpm}$ in Fig. 13 and 15. The first comparison between measured and simulated results using the first iron loss model, without considering the harmonics in the flux density, is presented in Fig. 13 and 14.

The results show a good match in the direction of the quadrature current and a nearly good match of the point of maximum efficiency. In the direction of the negative direct current the consistency of measured (black) and simulated (white) results is poor. The simulated efficiency is too high in the greatest part of the measurement and increases in the direction of the d-axis. This is a result of the underestimated losses in the field weakening area, which can be seen in Fig. 14. The measured and simulated data have a good match for high d- and q-currents but decreases in the partial load area. As shown in the simulated results the area of partial load is the most important area for the loss minimizing control, because in this are the iron losses are the dominant loss part, which has to be minimized.

Adding the iron losses produced by the harmonics in the flux density leads to a significant improvement of the data match. Especially the efficiency comparison in Fig. 15 shows an excellent match of the measured and simulated data. The point of maximum efficiency can be calculated more precisely. In particular field weakening area in negative d-axis show a high improvement comparing to the first approach with the iron loss model without harmonics.

Figure 16 presents the comparison between measured and simulated losses. This approach shows a good match between measured and simulated losses. Comparing to the first approach the losses increase in the whole dq-plane and are particularly severe in the field weakening area.

However this approach shows an overestimation of the iron losses near the d-axis. Building the difference of the two iron loss simulation approaches delivers the part of losses produced by harmonics in Fig. 17. The calculated iron losses increase in the negative d-axis, which is in contrast to the behavior of the flux linkage.

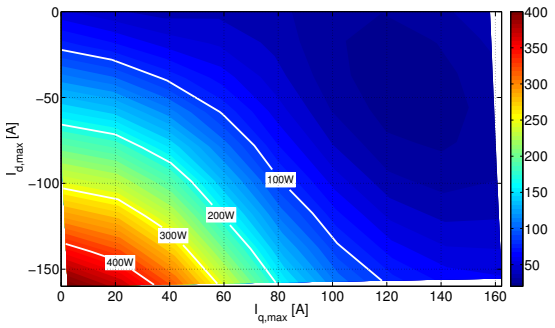

Fig. 17. Simulated iron losses caused by harmonics.

V. Conclusion

In this paper a methodology to reduce the overall losses in arbitrary operating points is proposed. Central part of this loss minimizing control strategy represents the simultaneous consideration of occurring copper losses and current dependent iron loss distribution. It is shown that this approach can be used to calculate the loss distribution *a priori* using iron loss models which are parameterized utilizing standardized Epstein measurement data. The used iron loss model is the most influencing parameter for the loss minimizing control strategy and should consider material saturation characteristics, rotational iron losses and harmonics to deliver reliable and accurate results in all operating points. The loss minimizing control reduces hysteresis losses by adding a direct or field weakening current component. This increases the ohmic losses but also the classical current losses, due to field harmonics, which has to be considered in the iron loss computation. In this paper an iron loss model is used, which considers the influence of induced field harmonics using a Fourier series representation of the magnetic flux density waveform for the least common multiple of an electrical period and the rotational period of the rotor. This approach shows a good validation with measured data. The interdependence of macroscopic and microscopic eddy currents, hysteresis, skin-effect and magnetic saturation significantly affects the field distribution within the lamination and as a consequence the overall iron losses and magnetizability. FE-Modells using the same BH-curve for all simulated frequencies do not consider the field and harmonics reducing skin-effect. In conclusion this approach shows a methodology for a priori loss prediction using standardized Epstein measurement data to parametrize iron loss models to obtain the current combinations, which minimize the overall losses in each operating point.

References

[1] F. Fernandez-Bernal, A. Garcia-Cerrada, and R. Faure, "Determination of parameters in interior permanent-magnet synchronous motors with iron losses without torque measurement," *Industry Applications, IEEE Transactions on*, vol. 37, no. 5, pp. 1265–1272, Sep 2001.

[2] G. xu Zhou, H. jun Wang, D.-H. Lee, and J.-W. Ahn, "Study on efficiency optimizing of pmsm for pump applications," in *Power Electronics, 2007. ICPE '07. 7th Internatonal Conference on*, Oct 2007, pp. 912–915.

[3] J. Lee, K. Nam, S. Choi, and S. Kwon, "A lookup table based loss minimizing control for fcev permanent magnet synchronous motors," in *Vehicle Power and Propulsion Conference, 2007. VPPC 2007. IEEE*, Sept 2007, pp. 175–179.

[4] M. Cao and N. Hoshi, "Electrical loss minimization strategy for interior permanent magnet synchronous motor drives," in *Vehicle Power and Propulsion Conference (VPPC), 2010 IEEE*, Sept 2010, pp. 1–6.

[5] J. Stumper, A. Dotlinger, J. Jung, and R. Kennel, "Predictive control of a permanent magnet synchronous machine based on real-time dynamic optimization," in *Power Electronics and Applications (EPE 2011), Proceedings of the 2011-14th European Conference on*, Aug 2011, pp. 1–8.

[6] T. Windisch and W. Hofmann, "Loss minimization of an ipmsm drive using pre-calculated optimized current references," in *IECON 2011 - 37th Annual Conference on IEEE Industrial Electronics Society*, Nov 2011, pp. 4704–4709.

[7] S. Odhano, R. Bojoi, A. Boglietti, G. Griva, and S. Rosu, "Maximum efficiency per torque direct flux vector control of induction motor drives," in *Energy Conversion Congress and Exposition (ECCE), 2014 IEEE*, Sept 2014, pp. 1293–1300.

[8] J. Goss, M. Popescu, D. Staton, R. Wrobel, J. Yon, and P. Mellor, "A comparison between maximum torque/ampere and maximum efficiency control strategies in ipm synchronous machines," in *Energy Conversion Congress and Exposition (ECCE), 2014 IEEE*, Sept 2014, pp. 2403–2410.

[9] J. Lee, K. Nam, S. Choi, and S. Kwon, "Loss-minimizing control of pmsm with the use of polynomial approximations," *Power Electronics, IEEE Transactions on*, vol. 24, no. 4, pp. 1071–1082, April 2009.

[10] C. Mademlis and N. Margaris, "Loss minimization in vector-controlled interior permanent-magnet synchronous motor drives," *Industrial Electronics, IEEE Transactions on*, vol. 49, no. 6, pp. 1344–1347, Dec 2002.

[11] D. Pohlenz and J. Bocker, "Efficiency improvement of an ipmsm using maximum efficiency operating strategy," in *Power Electronics and Motion Control Conference (EPE/PEMC), 2010 14th International*, Sept 2010, pp. T5–15–T5–19.

[12] C. Mademlis and N. Margaris, "Loss minimization in vector-controlled interior permanent-magnet synchronous motor drives," *Industrial Electronics, IEEE Transactions on*, vol. 49, no. 6, pp. 1344–1347, Dec 2002.

[13] H. Aorith, J. Wang, and P. Lazari, "A new loss minimization algorithm for interior permanent magnet synchronous machine drives," in *Electric Machines Drives Conference (IEMDC), 2013 IEEE International*, May 2013, pp. 526–533.

[14] A. Rabiei, T. Thiringer, and J. Lindberg, "Maximizing the energy efficiency of a pmsm for vehicular applications using an iron loss accounting optimization based on nonlinear programming," in *Electrical Machines (ICEM), 2012 XXth International Conference on*, Sept 2012, pp. 1001–1007.

[15] S. Steentjes, M. Lessmann, and K. Hameyer, "Advanced iron-loss calculation as a basis for efficiency improvement of electrical machines in automotive application," in *Electrical Systems for Aircraft, Railway and Ship Propulsion (ESARS), 2012*, Oct 2012, pp. 1–6.

[16] T. Herold, D. Franck, E. Lange, and K. Hameyer, "Extension of a d-q model of a permanent magnet excited synchronous machine by including saturation, cross-coupling and slotting effects," in *Electric Machines Drives Conference (IEMDC), 2011 IEEE International*, May 2011, pp. 1363–1367.

[17] F. Henrotte, G. Deliége, and K. Hameyer, "The eggshell approach for the computation of electromagnetic forces in 2D and 3D," *COMPEL*, vol. 23, no. 4, pp. 996–1005, 2004. [Online]. Available: http://134.130.107.200/uploads/bibliotest/2004FHelecmagn.pdf

[18] G. Bertotti, A. Canova, M. Chiampi, D. Chiarabaglio, F. Fiorillo, and A. Rietto, "Core loss prediction combining physical models with numerical field analysis," *Journal of Magnetism and Magnetic Materials*, vol. 133, pp. 647 – 650, 1994.

[19] F. Fiorillo and A. Novikov, "An improved approach to power losses in magnetic laminations under nonsinusoidal induction waveform," *IEEE Transactions on Magnetics*, vol. 26, no. 5, pp. 2904–2910, 1990.

[20] ——, "Power losses under sinusoidal, trapezoidal and distorted induction waveform," *IEEE Transactions on Magnetics*, vol. 26, no. 5, pp. 2559–2561, 1990.

[21] K. Grote and J. Feldhusen, *Dubbel: Taschenbuch für den Maschinenbau*. Springer Berlin Heidelberg, 2014.